Proceedings of the IASS 2024 Symposium
Redefining the Art of Structural Design
August 26-30, 2024, Zurich Switzerland
Philippe Block, Giulia Boller, Catherine DeWolf,
Jacqueline Pauli, Walter Kaufmann (eds.)

Topology optimization of trusses considering local buckling constraints of bars

Qi CAI [a,*], Yiyi ZHOU[b]

[a,*] College of Mechanics and Engineering Science, Hohai University, Nanjing, Jiangsu Province 211189, China
caiqi302@126.com

[b] College of Future Technologies, Hohai University, Nanjing, Jiangsu Province 211189, China

Abstract

For optimized truss structures to be practically applicable, it's essential to factor in the local stability of bars, ensuring stability and realism. Additionally, structural design must consider the initial crookedness of bars and residual stresses post-manufacture. These factors render the buckling strength highly non-convex and nonlinear concerning cross-sectional areas.Therefore, most conventional truss optimization formulations include only local buckling constraints based on the Euler buckling criterion, while local buckling constraints based on design codes are rarely incorporated. To treat these problems, a novel topology optimization formulation for trusses is proposed, where the critical buckling strength is calculated according to the practical design code GB5007-2017. In addition, a linearized iterative allowable stress method is used to solve the optimization model. Since the allowable stresses are calculated at each iteration based on the critical buckling strength, other types of design codes can also be incorporated into the proposed truss topology optimization model. The proposed computational model shows, through a numerical example, the remarkable effect of including local buckling stability in the optimal design of trusses, while demonstrating that the optimized topology depends on whether the local buckling constraints are derived from the Euler buckling criterion or from actual structural design codes.

Keywords: Local buckling; Truss; Topology optimization; Practical design code

1. Introduction

In conventional truss optimization models, the cross-sectional area of the bar typically serves as an optimization variable [1-6]. Moreover, since the critical buckling strength is contingent upon the cross-section's shape, this information must be incorporated. Specifically, the second moment of the cross-section is crucial for determining buckling strength. While simple cross-sections like circular or square ones allow for exact expression of the second moment of the area in terms of the cross-sectional area, the buckling strength itself is a concave function of the cross-sectional area [7, 8]. Consequently, obtaining optimal design becomes challenging.

Hence, many studies on optimizing truss structures overlook the local buckling issue of bars [9, 10]. To utilize the optimized structure in practical design, a common approach is to increase the cross-sectional area of buckling-prone bars post-optimization [11]. This transforms the nonlinear problem of truss optimization, considering bar buckling stability, into a linear optimization focusing solely on stress constraints. However, this method fails to consider bar local buckling stability during the optimization process, thus yielding suboptimal results. A basic strategy to address bar local buckling stability involves setting the allowable compression stress to a constant fraction of the tensile stress [12]. This results in unequal permissible stresses for tension and compression, eliminating the need for further adjustments for bar local stability. Nevertheless, selecting an appropriate constant lower stress constraint for bars

with varying lengths or axial forces proves challenging. Consequently, this method lacks practicality in integrating bar local buckling stability into truss optimization.

The Euler buckling criterion [13] is commonly integrated into truss optimization formulations due to its relatively straightforward expression. However, when employing the ground structure approach [14] using nested analysis and design formulation [15], incorporating Euler buckling constraints poses significant challenges. Notably, Euler buckling constraints exhibit behavior akin to stress constraints, notorious for rendering the feasible set non-convex [16] and inducing degenerate regions where optimal points may lie [17]. Moreover, the feasible set becomes disjointed with Euler buckling constraints. To address these issues, the ε-relaxed approach [18], adapted from a similar technique for stress constraints [19], can handle disjointness and degeneracy. Nonetheless, dealing with numerical challenges stemming from non-convexity and parameter ε selection persists. Additionally, this method may not yield satisfactory optimization results for pressure constraints.

Previous studies [13] have demonstrated that including local buckling in the truss optimization model can lead to vastly different topologies compared to those without such considerations. Hence, it is crucial to appropriately account for local buckling in truss optimization models. However, topology optimization of truss structures with bar buckling constraints based on design codes has received less attention compared to Euler buckling constraints. This is primarily due to the complexity of formulas in most design codes for calculating local buckling stability constraints, posing challenges for existing solvers. For instance, both Eurocode 3 [20] and GB5007-2017 [21] require consideration not only of bar length and cross-sectional shape but also of the slenderness ratio, further complicating the non-convex nature of the feasible set. Mela [12] proposed a mixed-variable approach incorporating bar local buckling stability constraints based on Eurocode 3 into truss topology optimization models. However, Mela's computational model relies on a computationally inefficient mixed-integer programming approach, limiting optimization to ground structures with few bars. Therefore, there is a need for a computationally efficient optimization model capable of directly incorporating design code buckling constraints.

In this study, we integrate the non-connected and non-convex local stability constraint into the truss topology optimization model using an iterative approach. Here, the local stability constraints undergo linearization and are tackled through a convex sub-problem. Furthermore, our formulation accommodates not only traditional Euler buckling constraints but also more intricate local buckling constraints derived from practical design specifications.

2. Equations

The truss optimization formulation included kinematic stability and bar local stability can be restated as,

$$
\begin{aligned}
\text{obj.}\quad & \min_{\mathbf{A},\mathbf{q}} \; M = \rho \mathbf{A}^{\mathbf{T}} \mathbf{L} \\
\text{s.t.}\quad & \mathbf{B}\left(\mathbf{q}_{+}^{k} - \mathbf{q}_{-}^{k}\right) = \mathbf{f}^{\mathrm{k}} \\
& -\sigma^{-} a_i \le q_{i,+}^{k} - q_{i,-}^{k} \le \sigma^{+} a_i \\
& \mathbf{B}\left(\mathbf{q}_{+}^{k+1} - \mathbf{q}_{-}^{k+1}\right) = \mathbf{F}_{\mathbf{X}} \\
& \mathbf{B}\left(\mathbf{q}_{+}^{k+2} - \mathbf{q}_{-}^{k+2}\right) = \text{-}\mathbf{F}_{\mathbf{X}} \\
& \mathbf{B}\left(\mathbf{q}_{+}^{k+3} - \mathbf{q}_{-}^{k+3}\right) = \mathbf{F}_{\mathbf{Y}} \\
& \mathbf{B}\left(\mathbf{q}_{+}^{k+4} - \mathbf{q}_{-}^{k+4}\right) = \text{-}\mathbf{F}_{\mathbf{Y}} \\
& \mathbf{F}_{\mathbf{X}} \ge r \mathbf{q}_{-}^{k} \mathbf{d}_{\mathbf{X}} \\
& \mathbf{F}_{\mathbf{Y}} \ge r \mathbf{q}_{-}^{k} \mathbf{d}_{\mathbf{Y}} \\
& a \le a^{cr} \\
& \mathbf{q}_{+}^{v},\ \mathbf{q}_{-}^{v} \ge 0 \\
& a_i \ge 0,\ q_{i,+}^{k} \ge 0,\ q_{i,-}^{k} \ge 0
\end{aligned}
\qquad
\begin{aligned}
& k = 1, 2, ..., N_f \\
& i = 1, 2, ..., N_b \\
& v = k{+}1, \ldots, k{+}2d
\end{aligned}
\qquad (1)
$$

where M is the mass of the structure, ρ is the density of the material (assumed same for all bars), $\mathbf{B} \in \mathrm{R}^{N_{dof} \times N_b}$ is the equilibrium matrix, built from the directional cosines of the bars, $\mathbf{q}_+^k \in \mathrm{R}^{N_b \times N_f}$ and $\mathbf{q}_-^k \in \mathrm{R}^{N_b \times N_f}$ are the matrixes containing the tension and compression forces under N_f external load conditions, respectively. Moreover, $\mathbf{f}^k \in \mathrm{R}^{N_{dof} \times N_f}$ is a matrix containing the external loads, $\sigma^+ > 0$ and $\sigma^- > 0$ are allowable tension and compressive stresses, respectively. $q_{i,+}^k$ and $q_{i,-}^k$ are the tension force and compression force of the bar i under loading case f^k. Moreover, $\mathbf{F_{X,Y}} = \left\{ \mathbf{F}_{\mathbf{X,Y}}^1, \mathbf{F}_{\mathbf{X,Y}}^2, ..., \mathbf{F}_{\mathbf{X,Y}}^{N_{dof}} \right\}^{\mathbf{T}}$ and, for a given node j, $\mathbf{F}_X^j = \left\{ f_X^j, 0 \right\}^{\mathbf{T}}$, $\mathbf{F}_Y^j = \left\{ 0, f_Y^j \right\}^{\mathbf{T}}$, where f_X^j and f_Y^j are the magnitudes of the nominal lateral force in the x- and y-directions. Further, $\mathbf{d_X}$ and $\mathbf{d_Y}$ are suitable $N_{dof} \times N_b$ matrices of bar cosines required to determine the component of compression force at each node perpendicular to the y- and x-axial respectively. r is the disturbing force coefficient, which takes the value 0.02 in this work. For the derivation of the formulations the reader is referred to the literature [22].

3. Iterative linearization algorithm

The critical buckling force exhibits concave behavior concerning the optimization variable, posing challenges for efficient results using conventional optimization solvers. Hence, we employ an iterative linearization algorithm to address this issue in solving the optimization formulation, outlined as follows:

(1) Solve the optimization problem (1) for axial forces (q_i) and sectional areas (a_i) for each bar. For the initial step, allowable tension stress σ^+ and compression stress σ^- for material should be used.

(2) For each compression bar i that is active in the optimized structure, use the axial force (q_i) to compute the critical buckling cross-sectional area ($a_i^{cr,s}$) and the total mass of structure M^s, where s is the current iteration count.

(3) For each compression bar i, calculate a new allowable compression stress value ($\sigma_i^{-,\,s+1}$). In order to provide a fully-stressed design, the value of the new stress is taken as

$$\sigma_i^{-,\,s+1} = \sigma_i^{-,\,s} \left(\frac{a_i^s}{a_i^{cr,\,s}} \right) \tag{2}$$

where $\sigma_i^{-,\,s}$ is the compression stress in the bar i at iteration s.

However, direct use of $\sigma_i^{-,\,s+1}$ in subsequent iterations is likely to cause cycling to occur if this is significantly different in magnitude to $\sigma_i^{-,\,s}$. Therefore, a relaxation term ζ, the value of which is to be taken between 0 and 1, is introduced in the calculation for $\sigma_i^{-,\,s}$. ζ has been taken as 0.5 for the problem described herein.

$$\sigma_i^{-,\,s+1} = \zeta \sigma_i^{-,\,s} \left(\frac{A_i^s}{A^{s,\,cr}} \right) + \left(1 - \zeta \right) \sigma_i^{-,\,s} \tag{3}$$

However, the stress $\sigma_i^{-,\,s+1}$ calculated by (3) may be larger than the allowable stress σ^-. Therefore, if $\sigma_i^{-,\,s+1} > \sigma^-$, then $\sigma_i^{-,\,s+1} = \sigma^-$ will be taken, that is

$$\sigma_i^{-,\,s+1} = \min \left(\zeta \sigma_i^{-,\,s} \left(\frac{A_i^s}{A^{s,\,cr}} \right) + \left(1 - \zeta \right) \sigma_i^{-,\,s},\ \sigma^- \right) \tag{4}$$

(4) Compare the previous value of structural mass M^{s-1}, M^{s-2}, M^{s-3} with this found in step (2), M^s. If $\Delta M \le \xi$, where $\Delta M = \left| \left(M^s + M^{s-1} \right) - \left(M^{s-2} + M^{s-3} \right) \right| \Big/ \left| M^{s-2} + M^{s-3} \right|$, convergence can be assumed to have occurred. ξ has been taken as 0.001 for the problem described herein.

(5) If the convergence criteria in step (4) are not met, redefine the allowable compression stress $\sigma^{-,s} = \sigma_i^{-,s+1}$ in accordance with formulation (4) and repeat from step (1).

4. Numerical examples

Two truss topology optimization examples are presented to illustrate the effectiveness of the method proposed in this study. The differences in the optimization results obtained based on the Euler buckling criterion and the structural design code GB5007-2017 are compared. The code is implemented in Matlab R2016b, and the LP solver is Mosek version 9.2.47. Mainly results are computed on a desktop with AMD Ryzen 7 2700X Eight-Core Processor 3.70 GHz and 32.0 GB of RAM.

4.1 Shell structure

As illustrated in Figure1a, the shell structure has a span of 32 m, height of 9.754 m, top sphere radius of 18 m, and bottom sphere radius of 17 m. Hinges constrain the bottom nodes of the top sphere, limiting horizontal and vertical movement. The design domain is subject to a vertically downward load conditions 2.5 kN/m² on the full span. For computational simplicity, uniform surface loads are transformed into concentrated loads on nodes based on load equivalence principles. Figure1b depicts the ground structure, featuring 241 nodes and 1,320 bars. The dome is symmetrically divided into 20 equal sections, generating a periodic design with a section angle of 18°. Cross-sectional areas and allowable stresses of bars at corresponding positions in each section are equalized for computational efficiency. Steel tubes are used as bars and only Euler buckling criterion constraint is considered. In addition, nominal lateral forces are not considered in the optimisation. Regarding material properties, Q355 steel is chosen with an allowable stress of 305 MPa and a Young's modulus of 210 GPa for this numerical example.

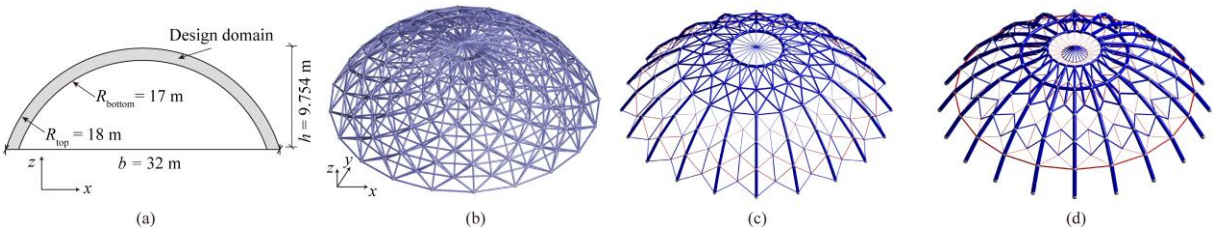

Figure 1 Optimized structures of the shell structure: (a) design domain, (b) Ground structure, (c) without local buckling stability constraint, (d) with Euler local buckling stability constraint.

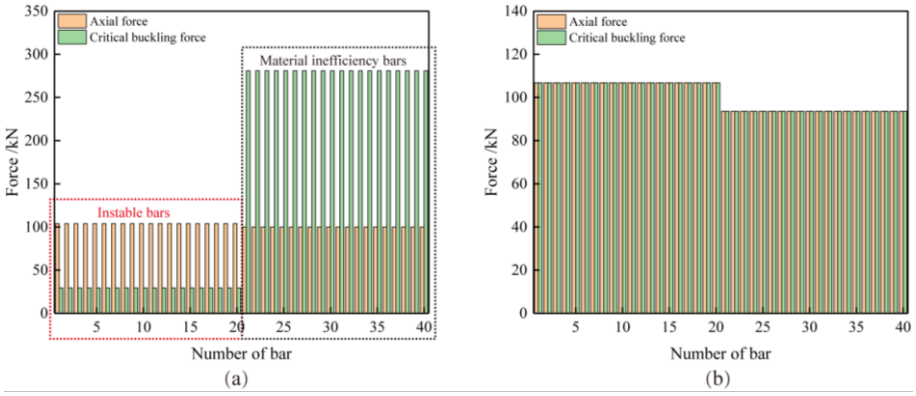

Figure 2: Comparison of axial force and critical buckling force of the compression bar: (a) without local buckling constraint; (b) with Euler local buckling stability constraint.

The optimized structure, without considering local buckling constraints, is depicted in Figure1c, featuring a mass of M_1 = 814.262 kg. The local stability information for the compression bars in Figure1c is shown in Figure2a, focusing on the axial forces and critical buckling forces of the 40 largest cross-sectional areas for clarity. Notably, some compression bars exhibit axial forces surpassing the critical buckling force, indicating instability. Conversely, several bars have axial forces significantly below the

critical buckling force, signifying material inefficiency. Subsequently, utilizing the algorithm proposed in this study to consider local buckling in the optimization, the resulting optimized structure is illustrated in Figure1d, with a mass of M_2 = 1,845.1 kg. Moreover, Figure2b displays the axial force and critical buckling force of the compression bars. Notably, all bars demonstrate local stability, affirming the effectiveness of the Iterative linearization algorithm.

4.2 L shape truss

As depicted in Figure 3, a typical 3D L-shape design domain (Figure 3a) provides a further indication of the range of applicability of the proposed approaches, where L is taken as 400 mm. Pinned supports are denoted by black dots on the top face, while two point loads P = 20 kN are applied downward at the tip of the 'L'.The design domain is discretized using 28 neighboring nodes connected by 138 potential straight bars to generate a ground structure (Figure 3b). For this numerical example, we utilize Q345 steel with the following specifications: allowable tensile and compressive stress of 305 MPa, yield stress of 345 MPa, density of 7.9 g/cm³, and Young's modulus of 206 GPa. The optimized structures are shown in Figure 3c-e. In addition, Figure 4 shows the comparison of axial force, Euler critical buckling force, and design code critical buckling force of the bar in the optimized structure. For clarity, only bars with a cross-sectional area exceeding 10% of the maximum cross-sectional area are indicated in Figure 4.

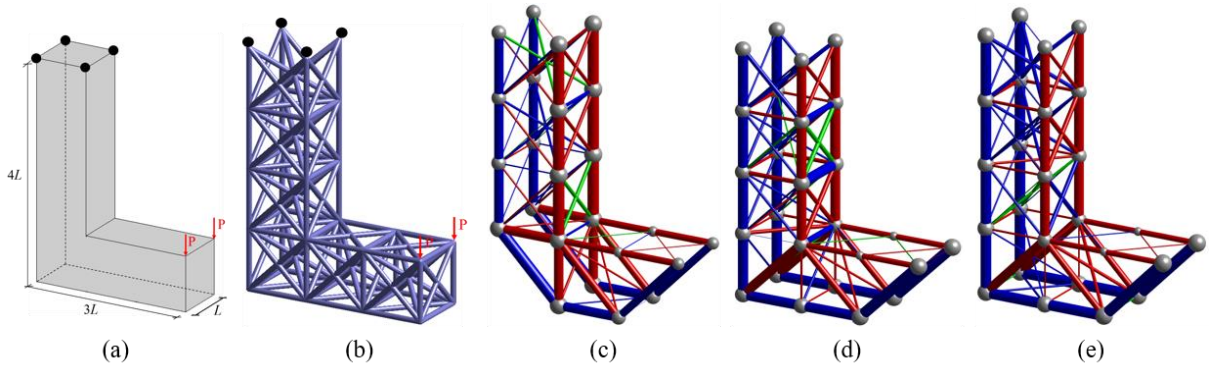

Figure 3 Optimization of L-shaped structure [27]: (a) Design domain, (b) Ground structure, (c) the optimized structure without local buckling stability constraint (OSWL), (d) the optimized structure with Euler local buckling stability constraint (OSEL), (e) the optimized structure with design code local buckling stability constraint (OSDL). The blue, red, and green lines represent the compressive bar, the tension bar, and the bar subjected to force only under the nominal perturbing force conditions, respectively.

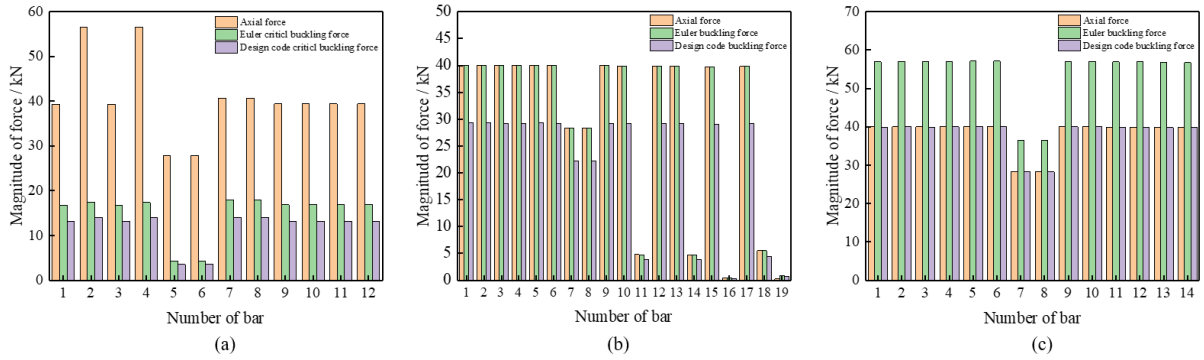

Figure 4 Comparison of axial force and critical buckling force of the optimized structure [27]: (a) optimized structure without local buckling stability constraint (OSWL), (b) optimized structure with Euler local buckling stability constraint (OSEL), (c) optimized structure with design code local buckling stability constraint (OSDL).

When neither the Euler local buckling nor design code local buckling constraint is considered in the optimization, the optimized structure (Figure 3c) with a mass of M_{OSWL} = 14.344 kg is obtained. However, as shown in Figure 3a, almost all of the bars do not meet either the Euler buckling requirements or the

structural design code requirements. Obviously, the optimization results cannot be directly used in the actual structural design.

As shown in Figure 3d, when only the Euler local buckling stability constraint is considered in the optimization, an optimized structure with a mass of M_{OSEL} = 21.584 kg is obtained, where $\left(M_{OSEL} - M_{OSWL}\right)/M_{OSWL} \times 100\% = 50.474\%$ more material is used to make the bar stable. However, as shown in Figure 4b shown, almost all of the bars do not meet the design code requirements. As shown in Figure 3e, an optimized structure with a mass of M_{OSDL} = 22.598 kg is obtained when the design code buckling stability constraint is considered. Comparing Figure 3d and Figure 3e, it can be seen that the topologies of the optimized structures based on Euler local buckling stability constraint and structural code local buckling stability constraint are different, which indicates that the optimization algorithm proposed in this study has the overall searching ability.

5. Conclusions

The primary contribution of this work lies in the proposal of a computational model incorporating bar local buckling stability constraints based on the practical design code GB5007-2017. In this truss optimization model, the cross-sectional area of the bar serves as the optimization variable, the mass of the structure is the optimization objective, and stress, nodal equilibrium, and bar local buckling stability serve as constraint conditions.

Furthermore, the integration of the bar local buckling constraint based on the practical design code renders the feasible set of design variables non-connected and non-convex, posing challenges for obtaining optimal solutions with existing solvers. To address this issue, a linearized iterative approach for modifying allowable stresses is proposed.

Finally, numerical examples illustrate that a significant portion of bars in the optimized structure, based on the Euler buckling criterion, fail to meet the requirements of practical design codes for local buckling stability. Additionally, the topology of the optimized truss varies depending on whether the buckling constraints are derived from the Euler buckling criterion or from design codes. Consequently, it is recommended to directly include local buckling constraints based on the design code in the truss topology optimization model.

Acknowledgements

This research is financially supported by the Jiangsu FundingProgram for Excellent Postdoctoral Talent.

References

[1] L. W. He, M. Gilbert, and X. Y. Song, "A Python script for adaptive layout optimization of trusses", *Structural and Multidisciplinary Optimization*, Article vol. 60, no. 2, pp. 835–847, 2019.

[2] F. Liu, R. Feng, K. D. Tsavdaridis, and G. Yan, "Designing efficient grid structures considering structural imperfection sensitivity," Engineering Structures, vol. 204, 109910, 2020.

[3] A. Kaveh and B. Ahmadi, "Sizing, geometry and topology optimization of trusses using force method and supervised charged system search," *Structural Engineering and Mechanics*, vol. 50, no. 3, pp. 365–382, 2014.

[4] A. Kaveh, B. Hassani, S. Shojaee, and S. M. Tavakkoli, "Structural topology optimization using ant colony methodology," *Engineering Structures*, vol. 30, no. 9, pp. 2559–2565, 2008.

[5] A. Kaveh and K. B. Hamedani, "Improved arithmetic optimization algorithm and its application to discrete structural optimization," *Structures*, vol. 35, pp. 748–764, 2022.

[6] A. Kaveh and A. Zaerreza, "A new framework for reliability-based design optimization using metaheuristic algorithms," *Structures*, vol. 38, pp. 1210–1225, 2022.

[7] H. Y. Cui, H. C. An, and H. Huang, "Truss topology optimization considering local buckling constraints and restrictions on intersection and overlap of bar members," *Structural and Multidisciplinary Optimization*, vol. 58, no. 2, pp. 575–594, 2018.

[8] G. I. N. Rozvany, "Difficulties in truss topology optimization with stress, local buckling and system stability constraints," *Structural Optimization,* vol. 11, no. 3-4, pp. 213–217, 1996.

[9] Y. Z. He, K. Cai, Z. L. Zhao, and Y. M. Xie, "Stochastic approaches to generating diverse and competitive structural designs in topology optimization," Finite Elements in Analysis and Design, vol. 173, 103399 ,2020.

[10] T. Zegard and G. H. Paulino, "GRAND3-Ground structure based topology optimization for arbitrary 3D domains using MATLAB," (in English), *Structural and Multidisciplinary Optimization,* Article vol. 52, no. 6, pp. 1161–1184, 2015.

[11] Topping and B. Hv, "Shape Optimization of Skeletal Structures: A Review," *Journal of Structural Engineering,* vol. 109, no. 8, pp. 1933–1951, 1983.

[12] K. Mela, "Resolving issues with member buckling in truss topology optimization using a mixed variable approach," *Structural and Multidisciplinary Optimization,* vol. 50, no. 6, pp. 1037–1049,2014.

[13] P. N. Poulsen, J. F. Olesen, and M. Baandrup, "Truss optimization applying finite element limit analysis including global and local stability", *Structural and Multidisciplinary Optimization,* Article vol. 62, no. 1, pp. 41–54, Jul 2020.

[14] W. Dorn, R. Gomory, and H. Greenberg, "Automatic design of optimal structures," *Journal de Mécanique,* vol. 3, pp. 25–52, 1964.

[15] J. S. Arora and Q. Wang, "Review of formulations for structural and mechanical system optimization," *Structural and Multidisciplinary Optimization,* vol. 30, no. 4, pp. 251–272, Oct 2005.

[16] A. Kaveh and A. Zolghadr, "Topology optimization of trusses considering static and dynamic constraints using the CSS," *Applied Soft Computing,* vol. 13, no. 5, pp. 2727–2734, May 2013.

[17] G. D. Cheng and X. Guo, "A note on a jellyfish-like feasible domain in structural topology optimization," *Engineering Optimization,* vol. 31, no. 1, pp. 1–24, 1998.

[18] X. Guo, G. Cheng, and K. Yamazaki, "A new approach for the solution of singular optima in truss topology optimization with stress and local buckling constraints," *Structural and Multidisciplinary Optimization,* vol. 22, no. 5, pp. 364–372, Dec 2001.

[19] G. D. Cheng and X. Guo, "epsilon-relaxed approach in structural topology optimization," *Structural Optimization,* vol. 13, no. 4, pp. 258–266, Jun 1997.

[20]Eurocode 3: Design of steel structures – Part 1–1: General rules and rules for buildings, 2005.

[21] Standard for design of steel structures (GB 5007-2017). Ministry of Housing and Urban-Rural Development of the People's Republic of China, China, Beijing, 2017.

[22] Q. Cai, R. Q. Feng, and Z. J. Zhang, "Topology optimization of trusses incorporating practical local buckling stability considerations," *Structures,* vol. 41, pp. 1710–1718, 2022.